

Article

Not peer-reviewed version

---

# Force in Cable of Pretensioner Tube – A Method of Car Accident Reconstruction

---

[Adrian Soica](#) \*

Posted Date: 18 March 2024

doi: 10.20944/preprints202403.0841.v1

Keywords: accident reconstruction; seat-belt; pbp and plp pretensioner; force-deformation polynomial regression; tube indentation



Preprints.org is a free multidiscipline platform providing preprint service that is dedicated to making early versions of research outputs permanently available and citable. Preprints posted at Preprints.org appear in Web of Science, Crossref, Google Scholar, Scilit, Europe PMC.

Copyright: This is an open access article distributed under the Creative Commons Attribution License which permits unrestricted use, distribution, and reproduction in any medium, provided the original work is properly cited.

*Article*

# Force in Cable of Pretensioner Tube—A Method of Car Accident Reconstruction

Adrian Soica

Department of Automotive and Transport Engineering, Transilvania University of Brasov, 500036 Brasov, Romania; a.soica@unitbv.ro

**Abstract:** The reconstruction of traffic accidents has grown as an interdisciplinary field since the first accident occurred. Various methods have been developed over time, starting with primary data collected at the scene of the accident. In this work, I proposed a method by which the value of the force in the safety belt buckle can be determined when it is equipped with a pretensioning system with pyrotechnic trigger in the tube, PBP or PLP type. The anti-return system of the pretensioner mechanism, which prevents the passenger's body from moving forward, contains a set of balls that block the movement of the piston in the pretensioner tube after its activation. When limiting the movement, the force the human body exerts on the safety belt webbing is transformed into the deformation of the pretensioner tube by the balls of the anti-return system. Depending on the magnitude of the force, the marks left by the balls differ. I propose a relationship of dependence between the acting force and the deformation of the tube. An experimental test bench was created to perform shock traction tests on the pre-tensioning system, under similar conditions to those of the human body acting on the belt in case of a frontal collision. Following the tests, the force value of the seat belt buckle cable and the diameter of the spherical indentations that the balls left in the pretensioner tube were measured. A mathematical model was proposed to determine the normal force with which a ball from the anti-return system deforms the tube. The normal force was also determined by two other methods specific to contact mechanics and used in the specialized literature. By comparing the normal forces obtained by the three methods, a good correlation between the proposed mathematical model and the Komvopoulos-Ye method resulted, the "Hardness" method not being suitable for this study. The determined polynomial regression curve allows finding out the force in the cable of the closer depending on the size of the deformations produced by the balls in the tube. The forces in the belt webbing can be thus determined and biomechanics specialists can evaluate the injuries to the chest and abdomen of the occupants of a vehicle.

**Keywords:** accident reconstruction; seat-belt; PBP and PLP pretensioner; force-deformation polinomial regression; tube indentation

---

## 1. Introduction

Vehicle accident reconstruction is a multidisciplinary field that often involves collaboration between, engineers, forensic experts, and law enforcement personnel. The goal is to piece together a comprehensive and accurate understanding of the traffic collision for safety and legal purposes. These techniques help investigators to determine factors such as the speed of the vehicles, point of impact, and the sequence of events. Some common car accident reconstruction techniques comprise:

Immediately after the accident, police officers take measurements and photographs at the accident site using topography equipment or laser scanners. They help create accurate, scaled sketches of the accident. Photogrammetry is a laboratory method that involves the analysis of images taken at the scene of the accident to create 3D models. These models can help determine vehicle positions, speeds and impact angles. This is done by technical experts who have access to the data collected by the police at the scene of the accident. Likewise, in the first stage after the accident, thorough examinations of the vehicles involved are carried out to assess damage patterns, tire marks and other physical evidence. This information helps determine the point of impact and the speed of the vehicles. The analysis is carried out by technical experts or forensic officers;

By studying skid marks, yaw marks, the scattering distance of the fragments and other tire impressions, experts can analyze the acceleration, deceleration, and braking behavior of the vehicles involved. This is one of the oldest methods of accident reconstruction; it is usually done immediately after the traffic accident;

An exact method of accident reconstruction is carried out in research centers approved by builders and various authorities in the field. Controlled crash tests using similar vehicles can help recreate and understand the collision in depth. These tests provide data that can be compared to the actual crash in order to validate reconstruction results, but they require expensive test facilities and precision equipment to measure and record the data. Computer software is used to create simulations based on available evidence. This includes inputting data such as vehicle speeds, impact angles, travel conditions of traffic participants, acceleration, deceleration, as well as road conditions (adhesion) to model the collision and its consequences. Various software applications such as Madymo, PC-Crash, Virtual Crash, PAM-Crash with powerful databases of vehicles and their occupants are used;

Many modern vehicles are equipped with event data recorders, which record various data points before, during and after an accident. For instance, this includes information about speed, brake status, throttle position and so forth. Key data may be downloaded by specialized personnel from these "black boxes" in the event of an accident. Analyzing the forces in a seatbelt involves understanding the physics of restraint systems during a vehicle collision. Seatbelts play a crucial role in protecting occupants by distributing and managing the forces generated during a crash. In a collision, the seatbelt applies force to restrain the occupants and prevent them from continuing to move forward.

During a collision, a vehicle undergoes rapid deceleration. Seatbelts are designed to slow down this deceleration experienced by occupants, spreading the forces over an extended period to reduce the risk of injury. Many modern seatbelts are equipped with load limiters. These devices allow a controlled amount of webbing to spool out during a collision, reducing the peak forces applied to the occupant. Pretensioners are devices that retract the seatbelt slightly during a crash, removing excess slack. The seatbelt webbing is a critical component in distributing forces. The tension in the seatbelt is carefully calibrated to manage the energy absorption during a collision while avoiding excessive loading on the occupant. Various safety standards and regulations establish performance criteria for seatbelt systems. Compliance with these standards ensures that seatbelts provide effective restraint during crashes.

Different seatbelt systems have been investigated for decades due to their potential for distributing belt forces and for providing alternative load paths for the head in both frontal and lateral impacts. [1] The space within the vehicle interior allows the restraint system to dissipate a larger amount of the occupant's energy during the collision event without the occupant being injured by the shoulder belt restraining load. [2]

The 3-point belt is a generally accepted and effective way to restrain vehicle occupants in case of a frontal impact. The overall lifesaving effectiveness was estimated to amount to 61% [3]. Nevertheless, performance can be improved. Pretensioned and force-limiting seat belts in combination with airbags were shown to significantly reduce thoracic loading and consequently thorax injuries for a driver [1,4,5]. As an output of the restraint system, the seat belt behavior can be influenced by different parameters; for example, occupant anthropometries, belt geometry, and crash severities [6].

The seatbelt provides initial restraint to the occupant body from the beginning of collision, while the airbag can distribute the restraining load over the chest. Accident data analysis shows a benefit of seatbelt load limiters in frontal collisions, and a load limiter value of 4kN was proposed to achieve a good balance with the airbag [7–9].

In [10,11] are presented studies on the dynamic deformations produced by spherical projectiles at high speeds. We consider that the level of energies produced during the interaction between the target and the projectile is much too high to make comparisons with the present situation, and

subsequently these studies are not suitable for determining indentations with much smaller dimensions as found in the case of pretensioning systems.

The aim of the paper is to determine the force in the buckle cable of the safety belt equipped with the PBP-Pyrotechnical Buckle Pretensioner or PLP-Pyrotechnical Lap Pretensioner system. The method is applicable in the case of a frontal impact of a vehicle by measuring the marks that the balls of the anti-return system of the pretensioner leave on the tube and the piston of the system. Once the tension in the buckle cable is established, the force in the seat belt webbing and its action on the occupant's chest and pelvis can then be determined. It is known that this depends on several factors previously mentioned and analyzed in various studies. Among these factors we mention: the anatomical constitution of the passenger, his age [12], the position of the driver [13], the intensity of the impact as well as the construction and adjustment method of the seat belt safety [6,14,15].

Thus, a new method is proposed to help in the reconstruction of traffic accidents, by analyzing the PBP type pretensioning mechanism of the safety belt, Figure 1. During a traffic accident, when the passengers are restrained with the seat belt, their forward body movement is limited by the belt webbing. The webbing is connected through the belt buckle, by means of a cable, to the piston of the mentioned system. The anti-return system of the pre-tensioning limits the movement of the passengers towards the dashboard. The force with which the passenger's body acts on the belt is transformed into the deformation of the tube pretensioner.



**Figure 1.** The PBP pretensioner, area of interest for proposed method.

Experimental tests were carried out on a specially designed installation, with various traction forces, using the pretensioning system from a safety belt with three-point attachment. The belt model in three points is, in accordance with the European Union's general approach to "Vehicles" in the Transatlantic Trade and Investment Partnership negotiations, equipped with PBP (Pyrotechnical Buckle Pretensioner). This document considers, as a test case, the US and EU legislation regarding seat belt anchorages. The presence of the occupant in the seat or on a special catapult-type stand is not necessary, because only the deformations in the PBP piston/cylinder (tube) pretensioning mechanism were analyzed. The goal is to make a correlation of these deformations with the force in the cable leading to the seat belt buckle. The distribution of effort on the two loops of the strap and the effects on the human body are not the subject of this study, some of these aspects being presented in various studies such as [12,16].



## 2. The Phenomenon Description and Used Methods

The pyrotechnic pretensioning systems, with cable, are found on the PBP and PLP models. In terms of location/position, they also coincide with the seat belt anchorage points in the area of the central tunnel of the body, respectively on the B-pillar, in the lower area. Their components include:

- The guide tube of the piston, which usually has a built-in pyrotechnic staple. It is the element that deforms in the process of blocking the anti-return system;
- The piston, mounted at the end of the belt buckle cable, for the PBP model. It is pushed by the force of the gases generated by the pyrotechnic staple and reduces the slack in the belt webbing. It has a special shape, geometry similar to a truncated cone, with generators inclined at approximately 7 degrees. Its shape allows blocking the reverse movement of the belt cable, after the pyrotechnic staple has been triggered.
- The balls of the anti-return system are mounted in a special plastic cage, similar to a bearing cage. Their arrangement is around the conical area of the piston, on its generators. They make contact with both the piston and the tube.

The process of blocking the pre-tensioning mechanism, type PBP, is carried out as follows:

- After activating the pyrotechnic staple and performing the tightening stroke of the seat belt on the occupant's body, the passenger tends to move forward due to inertia in the event of a frontal impact. At this moment the balls of the anti-return system come out of their resting position and tend to "climb" the conical surface from a smaller diameter to a larger one, until the moment when the piston-balls-cylinder mechanism stops;
- The intensity of the force with which the occupant's body acts on the belt straps will lead to the deformation of the piston and the cylinder, the balls leaving imprints in them, Figure 2.

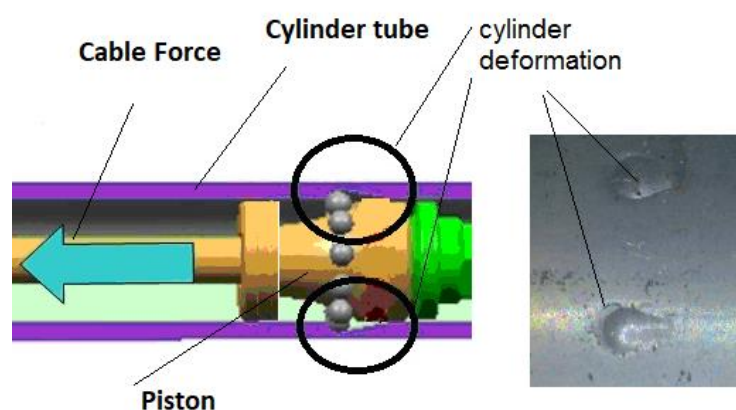


**Figure 2.** The functioning of the anti-return system for the PBP tube during the blocking of the pretensioning mechanism.

At the contact between the balls of the locking mechanism and the piston, respectively the cylinder of the pre-tensioning tube, normal reactions will occur on the surface of the piston and cylinder due to the traction force from the belt. These will cause the human body to stop advancing after pre-tensioning by deforming the material of the piston and cylinder.

We identify the situation of a spherical contact with indentation in plastic regime studied under various aspects in [17–22]. These were studied in numerous works, starting with the early years of the 20th century, for the development of models for testing the hardness of materials [23,25,26], as well as for the determination of spherical indentation in the elastic-plastic regime [24,27–29]. Throughout the time, the study of the indentation contact has attempted to develop models for testing material hardness. In the indentation models, contact between a rigid sphere and a deformable flat is considered as shown in Figure 2, where “N” is the normal force that acts on the indenter, “D” is the diameter of indenter, “d” is the diameter of indentation and “h” is the depth of indentation on flat wall. Points A, B and O define the angle “ $\varphi$ ” of spherical head, which is used to establish the depth

of indentation. The simplified diagram of the plastic deformation mechanism of a straight surface under the action of a normal force is presented in Figure 3.

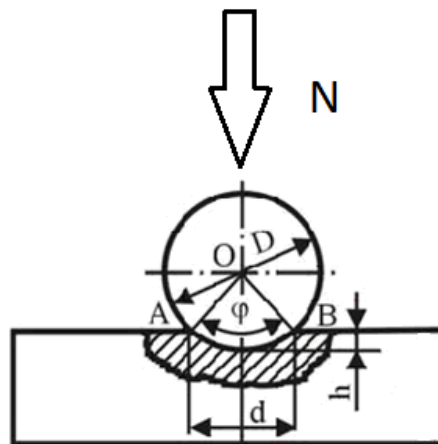


**Figure 3.** Normal force and deformation occurring at the contact between the balls and the cylinder/piston.

If the pulling force, generated by the movement of the passenger's body, is high, settlement deformations can also occur on a certain length of the cylinder generator, Figure 3. In the proposed model, the tangential acting force is given by the force with which each ball acts on the tube. Figure 4b shows the traces left by the balls on the cylinder wall during the blocking of the pretensioning mechanism.

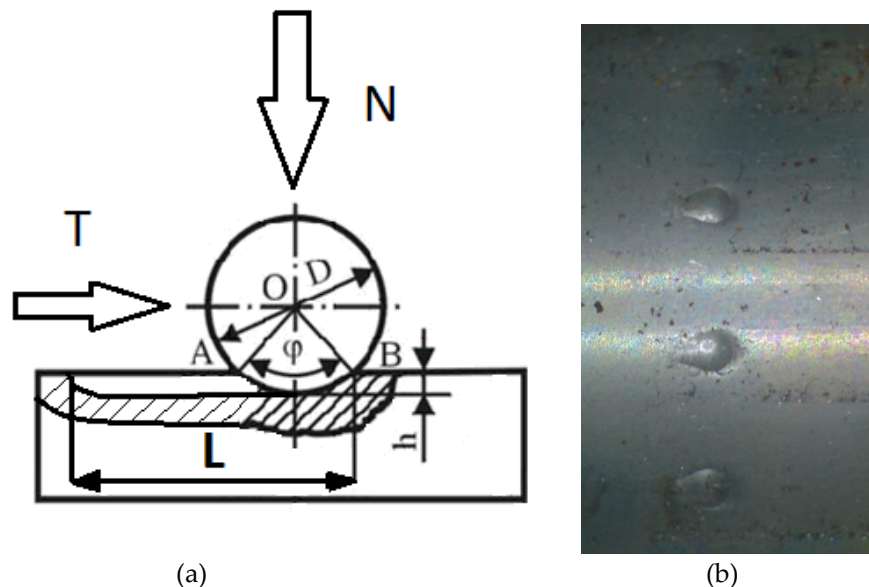


**Figure 4.** Deformation by settling along a certain length, a - schema, b – real.

The presence or absence of a webbing force limiting mechanism (RLE) and the magnitude of the force at which this system comes into action, influences the way the cylinder is deformed by the locking balls. Figure 5 shows the sectioned tube of the pretensioning system, after being acted upon with the traction force of the cable written here as " $F_{\text{cable}}$ ". Also, as it can be seen, the ball cage, which holds the balls on the tube generator and piston, the piston and the cable crimp on the cable end. By analyzing the marks left by the balls in the cylinder and in the piston, Figure 4, the diagram of the forces acting on the anti-return system of the PBP type pretensioning mechanism can be drawn up.



**Figure 5.** Example of cylinder deformed following the functioning of the anti-return pretensioning mechanism PBP.

### 3. The Models

Three mathematical models, one model proposed by the author and two models taken from the literature have been used to determine the normal force with which the ball acts on the tube of the pre-tensioning system. The force values have been compared in order to validate the results.

#### 3.1. Proposed Model

The diagram depicted in Figure 6 shows the forces acting on the anti-return system, which is composed of a piston-ball-tube, in the stage of blocking the passenger's movement due to inertia. Through the movement of the piston, given by the force in the cable " $F_{cable}$ " generated by the human body, the ball moves on the shape of the inclined plane of the piston and comes into contact with the piston and the tube of the pretensioner, causing the system to block and the deformation of these components which have a much higher hardness small. Basically, the ball has the role of a feather. From the balance of the forces on the X and Y axes it follows (the forces corresponding to the action of the ball on the cylinder and the piston have been illustrated).

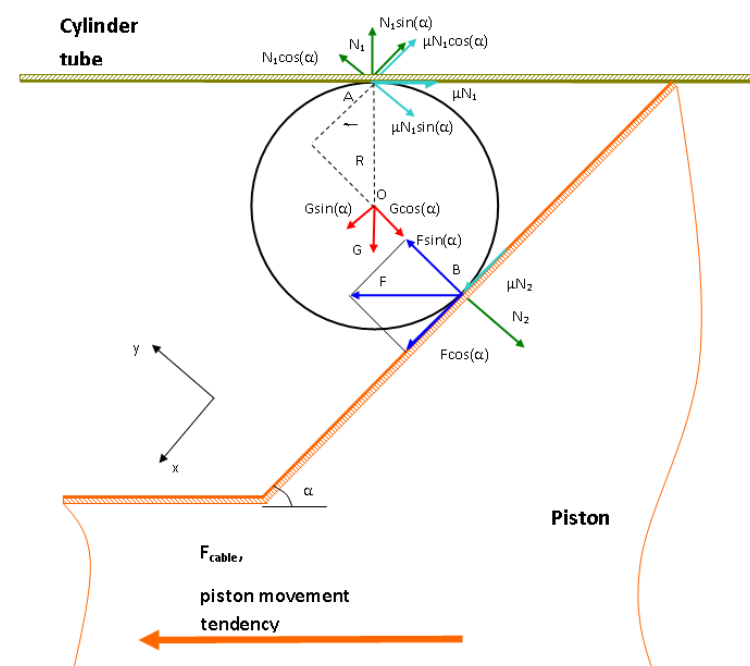


**Figure 6.** Diagram of forces for the mathematical model proposed.

The force acting on a ball is given by the ratio of the force in the traction cable to the number of balls mounted on the piston generator:

$$F = \frac{F_{cable}}{n} \quad (1)$$

$$F \cdot \cos(\alpha) + \mu_2 \cdot N_2 + m \cdot g \cdot \sin(\alpha) - N_1 \cdot \sin(\alpha) - \mu_1 \cdot N_1 \cdot \cos(\alpha) = 0 \quad (2)$$

$$F \cdot \sin(\alpha) - N_2 - m \cdot g \cdot \cos(\alpha) + N_1 \cdot \cos(\alpha) - \mu_1 \cdot N_1 \cdot \sin(\alpha) = 0 \quad (3)$$

By writing the moments relative to point A or B we have

$$m \cdot g \cdot \sin(\alpha) \cdot r \cdot \cos(\alpha) + F \cdot \cos(\alpha) \cdot r \cdot (1 + \cos(\alpha)) - m \cdot g \cdot \cos(\alpha) \cdot r \cdot \sin(\alpha) + \dots + F \cdot \sin(\alpha) \cdot r \cdot \sin(\alpha) - N_2 \cdot r \cdot \sin(\alpha) + \mu_2 \cdot N_2 \cdot r \cdot (1 + \cos(\alpha)) = 0$$

(4)

$$m \cdot g \cdot \sin(\alpha) \cdot r - \mu_1 \cdot N_1 \cdot \sin(\alpha) \cdot r \cdot \sin(\alpha) - \mu_1 \cdot N_1 \cdot \cos(\alpha) \cdot r \cdot (1 + \cos(\alpha)) + \dots + N_1 \cdot \cos(\alpha) \cdot r \cdot \sin(\alpha) - N_1 \cdot \sin(\alpha) \cdot r \cdot (1 + \cos(\alpha)) = 0$$

(5)

The reaction forces,  $N_1$  and  $N_2$ , which cause the deformation of both the cylinder and the piston, are determined from relations (4) and (5). The friction coefficient between the ball and the piston, respectively the pretensioner tube, is chosen, in accordance with the data from [30–32], at a value of 0.15–0.2. It depends on the contact pressure between the two materials as well as on the sliding speed between them. As the speed and contact pressure increase, the friction coefficient decreases [33].

### 3.2. Determining the Normal Force of Action through the Hardness Method

Knowing the hardness according to Brinell method [25] of the piece in which the ball of diameter "D" left its mark and having the diameter "d" of the spherical indentation, the force with which the piece was acted upon can be determined, using a reasoning similar to the one applied to hardness determination by Brinell method. According to the diagram depicted in Figure 3, the value of the normal force of action is given by relation (7).

$$HB = \frac{2 \cdot N}{\pi \cdot D \cdot \left( D - \sqrt{D^2 - d^2} \right)} \quad (6)$$

Wherein

$$N = \frac{\pi \cdot D \cdot HB \cdot \left( D - \sqrt{D^2 - d^2} \right)}{2} \quad (7)$$

The angle of the spherical cap that penetrated the material can be obtained from the triangle OAB, Figure 2

$$\sin\left(\frac{\varphi}{2}\right) = \frac{\frac{d}{2}}{\frac{D}{2}} \quad (8)$$

wherein the depth with which the ball penetrates the material is determined from the triangle AOB and is described by the relationship:

$$h = \frac{D}{2} - \frac{D}{2} \cdot \cos\left(\frac{\varphi}{2}\right) \quad (9)$$

The value of the normal force, which deforms the tube, described by relation (7) is compared with that of the theoretical model given in relations (4) and (5).

### 3.3. Plastic Regime with Spherical Indentation



Determining the normal force of action by the method described in [17] requires knowledge of the material properties,  $E$  – Young modulus,  $S_y$  – yield strength and Poisson ratio, for the ball with the role of the spherical indenter and the cylinder with the role of the part where the deformation takes place.

$$\frac{1}{E} = \frac{1-\nu_1^2}{E_1} + \frac{1-\nu_2^2}{E_2} \quad (10)$$

$$\frac{1}{R} = \frac{1}{R_1} + \frac{1}{R_2} \quad (11)$$

A dimensionless factor is defined

$$Q = \frac{E}{S_y} \cdot \frac{h}{a'} \quad (12)$$

Where:

$$a' = \sqrt{\left(\frac{D}{2}\right)^2 - \left(\frac{D}{2} - h\right)^2} \quad (13)$$

$$A' = \pi \cdot a'^2 \quad (14)$$

$$\frac{A'}{A} = 0.05 \cdot (\ln Q)^2 - 0.57 \cdot (\ln Q) + 2.41 \quad (15)$$

When  $Q > 1.78$ , the elastic-plastic small deformation phase persists until  $Q \leq 21$ . For  $21 < Q \leq 400$ , the contact occurs in the elastic-plastic medium deformation phase and it has been considered to be consistent with the conventional hardness relation (note that this is the value assumed in their model). When  $Q > 400$  the contact is in elastic-plastic large deformation phase [17].

Depending on the value of  $Q$ , for the cases analyzed, according to [17]

$$\frac{N}{A} = 2.9 \cdot S_y \quad (16)$$

Hence, the value of the normal force  $N$ , which is compared with the one obtained from solving the system given by relations (4) and (5).

### 3.4. Virtual CAD-3D Models

Through CAD-3D modeling, the penetration depth of the ball can be determined virtually on surfaces with different geometries, depending on the diameter of the imprint. Thus, we modeled two surfaces, Figure 7, one flat and one cylindrical respectively, on a 1:1 scale, with the aim of determining the penetration of the ball into the material of the cylinder/flat surface, depending on the diameter of the measured imprint that the ball of the anti-return system leaves when the locking mechanism is blocked. The elliptical shape of the imprint left by the ball on the surface of the cylinder is observed, as opposed to the circular shape, in the case of the flat surface. As the curvature of the surface tends to infinity (flat surface), at the same depth of penetration, a smaller diameter of the imprint will result, and the shape tends to undergo an elliptical-to-circular transition.

Table 1.

Item	Plane Surface		Cylindrical Surface		
	h	d	h	d1	d2
1	0.05	0.76811	0.05	0.83840	0.76811
2	0.1	1.07702	0.1	1.1742	1.07702
3	0.15	1.30767	0.15	1.41726	1.30767
4	0.2	1.49666	0.2	1.61644	1.49666
5	0.3	1.80	0.3	1.93071	1.80

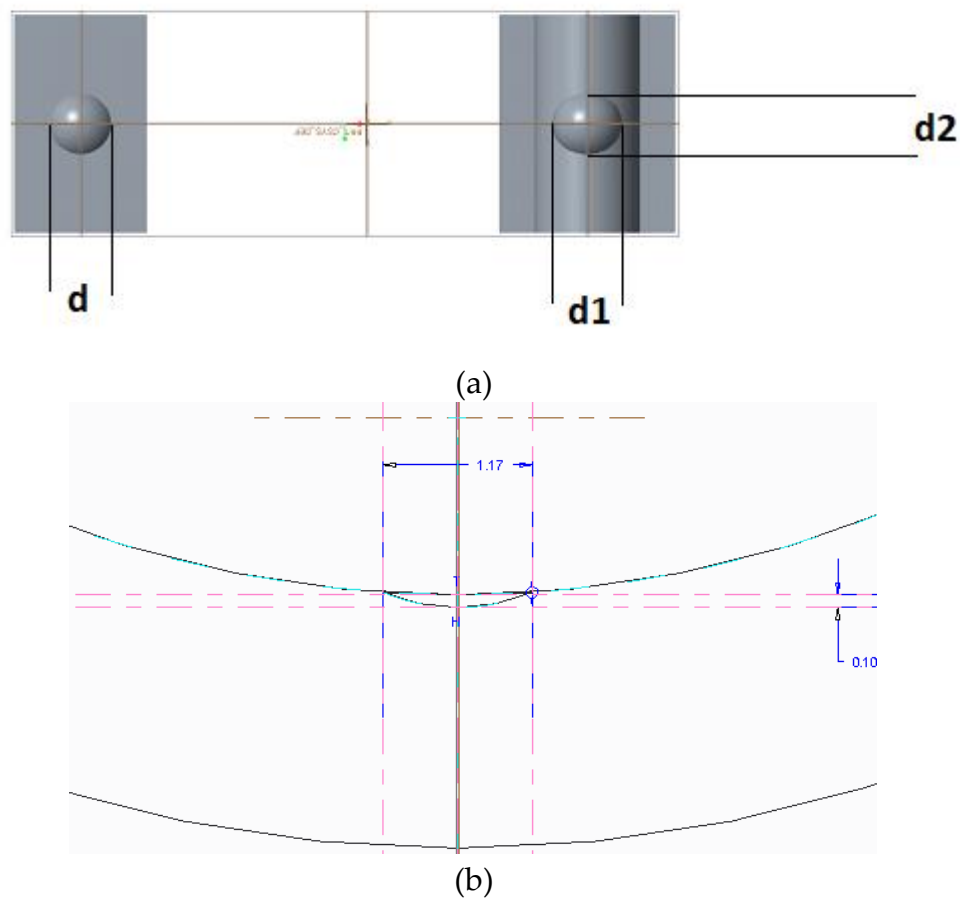


**Figure 7.** Shape of indenters on both flat and cylindrical surfaces (a), image size increased on the penetration depth of the spherical indenter in the virtual model (b).

#### 4. Experimental Setup

The experimental tests were done on a test rig shown in Figure 8. A system with a spring is used to simulate the resistance of the human body and the force with which it acts on the safety belt strap with the body area (chest in particular). The PBP type pretensioning system is fixedly mounted, maintaining the angle that the pull cable of the closer has when mounted on the vehicle. The main geometric characteristics and properties of the materials are:

- The tube of the pretensioning system has an inner diameter of 18 mm;
- The ball of the anti-return system has a diameter of 3 mm;
- The material of the tube is carbon steel EN 10305-1 or ISO 33044, with hardness HB 149;
- The ball is made of stainless steel X46Cr13, ISO 3290-1 or EN 10088, with a hardness of 56 HRC;

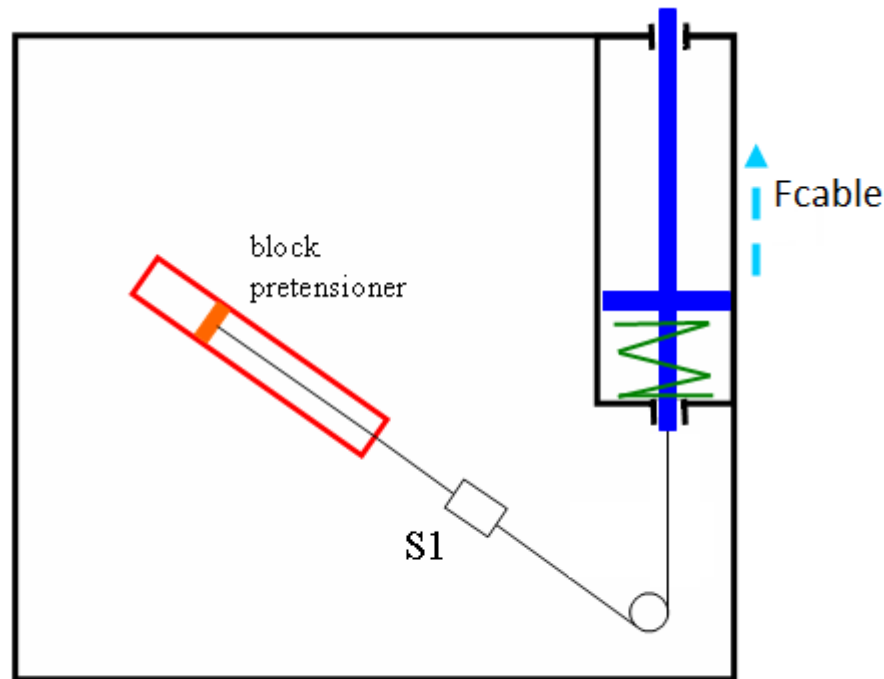


Figure 8. Experimental test rig schema.

A HBM C9C – 20 kN force transducer was mounted on the traction cable, at a sampling frequency of 4800 Hz. In the first phase, the pyrotechnic system is triggered, which develops a pulling force on the buckle's seatbelt cable. During this time, the displacement of the piston in the tube of the pretensioning system occurs. The second stage of the tests, in which the pretensioner is blocked and the marks left by the balls in the system tube appear, begins when the passenger's body (with the chest and pelvis area), due to the inertia and intensity of the impact, pulls the webbing, therefore the cable traction with " $F_{cable}$ " force. During the tests, the human body was replaced with a compressed spring. The energy accumulated is released upon decompression and it subsequently acts on the pretensioning system, which, through the mounted anti-return balls, blocks the release (unwinding of the strap). In real accidents, this blocking is translated by preventing the passenger from moving from the vehicle towards the dashboard.

The force developed in this stage, " $F_{cable}$ ", acts on the occupant's chest and pelvis. If a certain value is exceeded, the seat belt can trigger a limitation of the effort on the chest. The force values of the force limitation system (RLE) are set by the seat belt manufacturer, depending on the vehicle manufacturer's requirements. The tension limiting force on the passenger's body, in most types of safety belts used, can be constant, progressive or degressive. The threshold value at which the RLE system is activated is between 2-4 kN. In this way, less severe injuries may occur to the occupant's chest.

## 5. Discussion

The acting force in the safety belt buckle cable is divided into "n" forces that act on the balls kept equidistant through a special cage, all around the tube generator, Figure 5. The present analysis considers the force in the cable equally distributed on the number of balls. The acting time of the force in the cable differs depending on tests, considering the degree of compression of the spring, but we can say that it is approximately 10 ms, Figures 9–11. The deformation produced in the pretensioner tube is two-fold, under the action of both normal and tangential forces, a fact due to both the geometry of the parts and the acting force in the cable. The indentation left by a ball in the tube takes the form of a drop. The marks left by the balls on the tube generator have been compared and deviations of up to 10% of the measured diameters have been found. For the proposed mathematical

model, during the action of the force, it is considered that only the tube deforms plastically. The accuracy of the obtained results can be influenced by the characteristics of the materials in contact.

Thus, elastic deformation in the spherical indenter can cause prediction errors of up to 12%, as shown in [34]. Tabor [35] suggested that the yield strength of a spherical indenter should equal 2.5 times that of the flat indenter to prevent plastic deformation of the indenter. For the steel ball,  $S_y$  is approximately 650 MPa, and for the tube material it reaches 350 MPa [36].

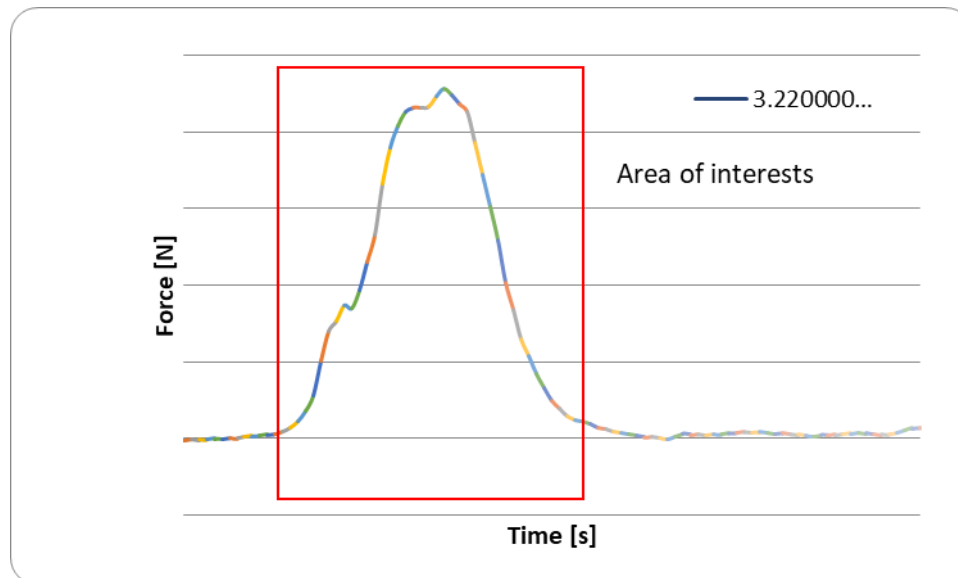


Figure 9. Force acting on buckle cable, sample test 11.

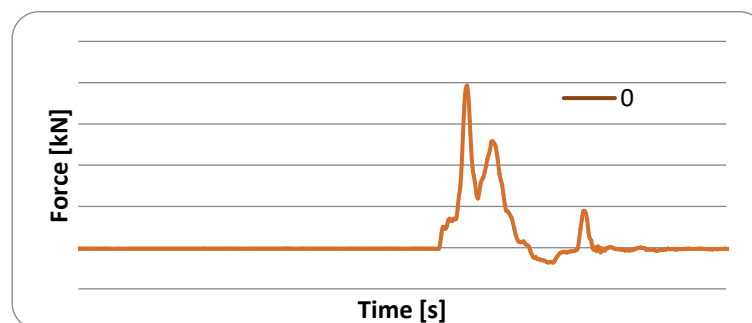


Figure 10. Cable force sample for test 4.

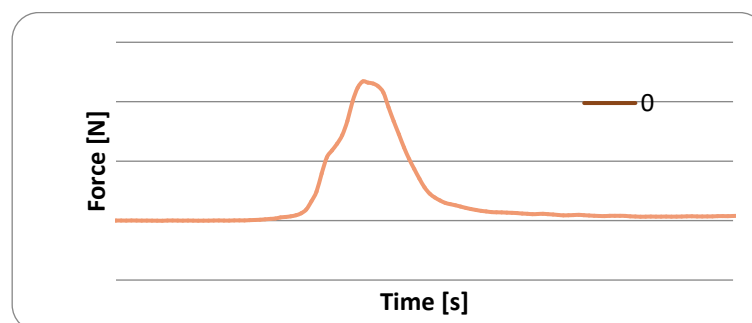


Figure 11. Cable force sample for test 5.

Eleven experimental tests were performed, with various action forces in the shutter cable. In the case of test no. 4, Figure 10, the values cannot be used because of the displacement/movement of the tube while the force is acting in the cable, it did not remain firmly fixed, thus the force at the moment 0.81 seconds shows two humps, unlike the other cases, Figure 11.

Values of forces measured and dimensions of marks are given in Table 2.



**Table 2.** Data about values of forces, indentation diameters and depths.

No. test	Force by [17]	Force by Harness method	Force by Mathematical model N1	Cable force experimental	Indentation Diameter experimental	Indentation depth experimental
	[N]	[N]	[N]	[N]	[mm]	[mm]
P1	549.192	767.198	623	1070	0.81	0.0557
P2	661	910.81	708.3	1138	0.881	0.0661
P3	1149	1533	1261.3	2210	1.134	0.111
P4	-	-	-	-	-	-
P5	745.17	1019	841.69	1344	0.93	0.074
P6	1144	1526	1261.97	2020	1.131	0.111
P7	1212	1612	1126.01	1798	1.162	0.117
P8	1397	1847	1491.11	2381	1.24	0.134
P9	725.1	993.104	805.411	1286	0.919	0.0721
P10	909.538	1228	905.62	1446	1.019	0.089
P11	1397	1847	1383.29	2209	1.24	0.134

After performing the tensile tests, in a first step, the dimensions of the spherical indentations obtained through the virtual CAD-3D model were compared with those obtained after the experiments. In Figure 12 we have represented the values of the diameters that define the elliptical shape of the indentation on the curved surface, together with their two trendlines. Following the experiments, the shape of the indentations marks in the tube was predominantly close to the diameter "d2" of indentation, their size fitting in the corridor defined by the two trend line curves. From the microscopic analysis, it was not possible to highlight the elliptical shape of the deformation, most plausibly due to the deformation process under the action of a normal force as well as the tangential one.

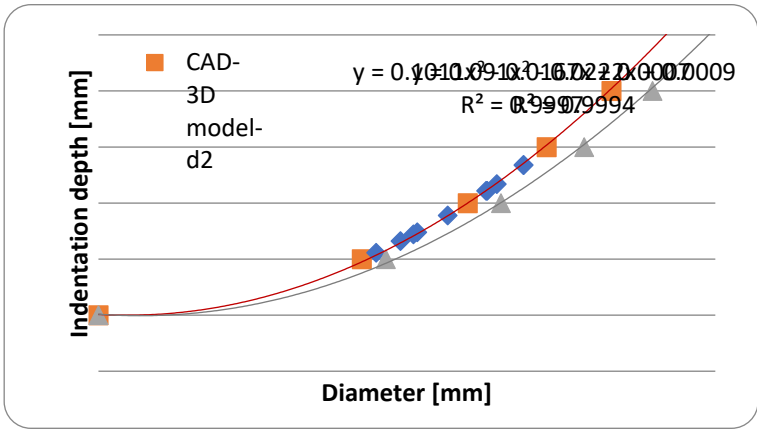


**Figure 12.** Values of diameter indentation for 3D model and experimental data.

Thus, a good correlation is observed, the deviations, insignificant, observed probably due to the measurement errors of the indentation diameters, prompted us to proceed to the stage of determining the forces. The values of the indentation depth were determined by calculation with relations (8) and (9).

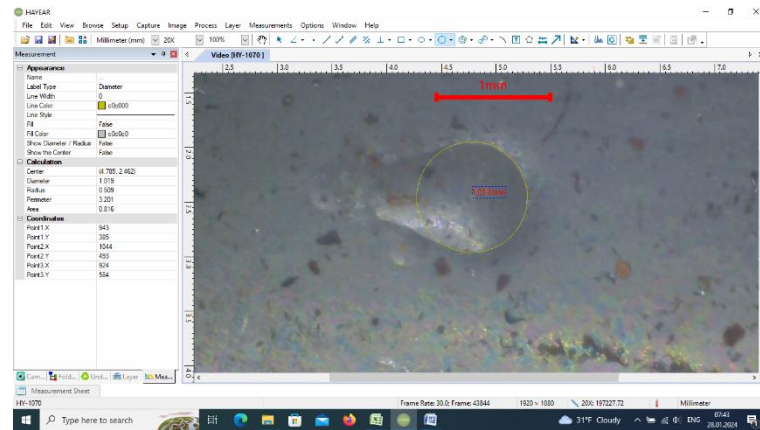


**Figure 13.** Sample of diameter measure based on experimental data.

In the next stage, the normal forces with which the balls act on the cylinder are compared by using three methods:

- the mathematical model proposed in this study;
- the "hardness" model;
- the Komvopoulos-Ye model, described in [17,28,29].

The force in the cable, obtained experimentally, was calculated as the average of the values over its range of action, see Table 2. These values cover the 1000-2400 N range, mostly up to the limit in which the effort limiter in the safety belt retractor would come into operation. The normal force with which the ball acts on the tube is determined, in the proposed mathematical model, starting from the force value measured in the belt buckle cable. The force values are lower than those determined by the "hardness" method. There is a good grouping of the values along a trend line (blue line). The coefficient of determination ( $R^2$ ) is 0.977, Figure 14.

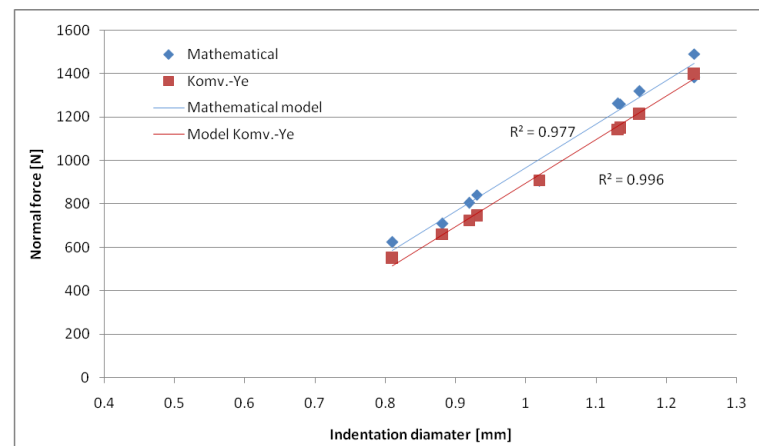


**Figure 14.** Normal forces for proposed model and elastic-plastic model, as function of indentation diameter.

In the model described in [17], the value of the normal force that produces the indentation has more grouped values compared to the trend line (red line), the coefficient of determination ( $R^2$ ) being in this case 0.996, Figure 14. The values of the forces are the lowest, by comparison with the other models wherein they were determined.

Between the proposed method and the one in [17], the ratio between the normal forces that deform the tube is between 0.99 and 1.134. Comparing the two trendlines, it is found that they are theoretically parallel, showing the same tendency, with the difference between the values of the forces slightly larger towards the small values of the indentation diameter and decreasing towards the larger diameters. In Figure 15 a comparison of proposed method and elastic-plastic spherical indentation model is presented.

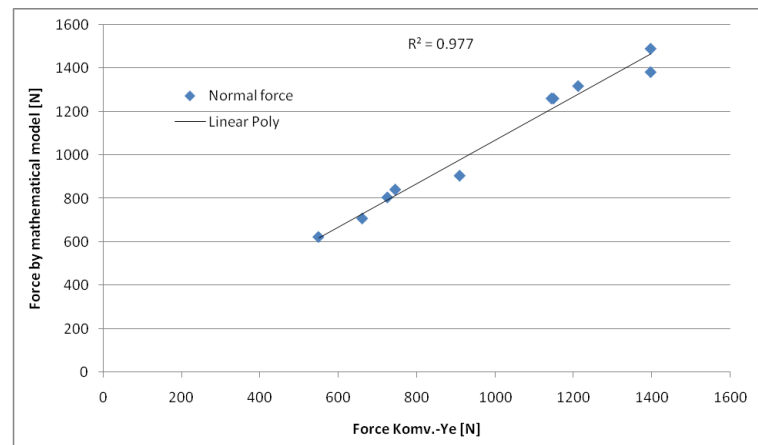


**Figure 15.** Comparison between proposed model and elastic - plastic model.

The normal strength values, obtained through the "hardness" method, are the highest, with variations of 32-40% compared to those resulting from the Komvopoulos-Ye method. Moreover, this is considered outdated in contact mechanics for the purpose of determining the plastic deformations of materials [17] and, therefore, we do not consider this method useful for the present case. The technical or judicial expert in traffic accidents can have easy access to the safety belt pre-tensioning system. In the case of a PBP or PLP type system, data can be obtained about the size of the indentations that the balls of the anti-return system have made in the tube. Based on a regression curve, the dependence between the force in the cable and the size of the mark can be determined with the traction force from the safety belt.

Thus, in the last stage of the analysis, we propose to establish a polynomial curve by which it is proposed to approximate the force in the cable of the seat belt buckle depending on the diameter of the mark left by the balls of the locking system in the pretensioner tube, Figure 16. The coefficient of determination ( $R^2$ ) is 0.92, which authorizes us to consider that in this way a good prediction can be made for the establishment of this useful force in the reconstruction of traffic accidents, starting from the marks left by the balls of the anti-return system during the traction appearing in the safety belt buckle cable.

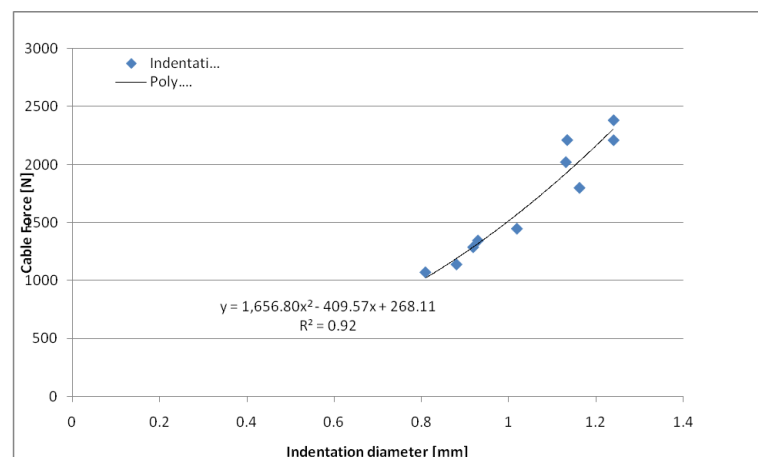


**Figure 16.** The proposed regression curve Force - Indentation.

## 6. Conclusions

The method can provide information for the analysis and reconstruction of traffic accidents by establishing the force with which the passenger's body acts on the seat belt buckle at the time of impact. This data can help to further determine the intensity of the frontal impact and the forces on the occupant's torso, especially at the level of the ribcage. The determination of the forces with which

the spherical indenter acts on the tube of the pretensioning system has been carried out by using three methods.

The proposed mathematical model and the method described in [17] show close results, the difference between not exceeding 10%. We believe that the model based on hardness measurement is not feasible for this type of analysis. A polynomial regression function, with a coefficient of determination ( $R^2$ ) = 0.92, based on the results of experimental tests, was proposed to establish the traction force in the seat belt buckle cable, depending on the deformations in the tube of the PBP pretensioning system.

**Author Contributions:** Conceptualization, A.S.; methodology, A.S. software, A.S.; validation, A.S. ; formal analysis, A.S.; investigation, A.S.; resources, A.S.; data curation, A.S.; writing—original draft preparation, A.S.; writing—review and editing, A.S.; visualization, A.S.; supervision, A.S.; project administration, A.S. All authors have read and agreed to the published version of the manuscript.

**Funding:** This research received no external funding.

**Data Availability Statement:** Not applicable.

**Conflicts of Interest:** The authors declare no conflict of interest.

## References

1. Kent, Richard; Lopez-Valdes, Francisco J; Dennis, Nate J; Lessley, David; Forman, Jason; et al. Assessment of a Three-Point Restraint System with a Pre-tensioned Lap Belt and an Inflatable, Force-Limited Shoulder Belt, *Stapp Car Crash Journal*; Ann Arbor 55, **2011**: 141-59.
2. Mertz, Harold J; Dalmotas, Dainius J. Effects of Shoulder Belt Limit Forces on Adult Thoracic Protection in Frontal Collisions, *Stapp Car Crash Journal*; Ann Arbor 51, **2007**: 361-80.
3. Cummings P, Wells JD, Rivara FP. Estimating seat belt effectiveness using matched pair cohort methods. *Accid Anal Prev.* **2003**;35:143–149.
4. Manuel Valdano, Jesús R. Jim'enez-Octavio , Francisco J. Lopez-Valdes , The effect of seatbelt pretensioners and load limiters in the reduction of MAIS 2+, MAIS 3+, and fatal injuries in real-world frontal crashes, *Accident Analysis and Prevention* 190, **2023**, 107180., <https://doi.org/10.1016/j.aap.2023.107180>
5. Bengt Pipkorn, Francisco J. López-Valdés, Oscar Juste-Lorente, Ricardo Insausti, Christer Lundgren, and Cecilia Sunnevang, Assessment of an innovative seat belt with independent control of the shoulder and lap portions using THOR tests, the THUMS model, and PMHS tests, *Traffic Injury Prevention*, **2016**, vol 17, No S1, 124-130
6. Mackay G, Hill J., The limitations of current seatbelts in Europe—some population considerations. *J Trauma.* , **1995**;38:533–537.
7. Lu H, Andreen M, Fausst D, Furton L, Holcombe S, Kohoyda-Inglis C, Putala B, Yee J, Wang S, Safety Belt and Occupant Factors Influencing Thoracic & Upper Abdominal Injuries in Frontal Crashes, Society of Automotive Engineers, inc., 2011-01-1129, 2011.
8. Foret-Bruno J-Y, Trosseille X, Le Coz J-Y, Bendjellal F, Steyer C, Phalempin T, Villeforceix D, Dandres P, Got C. Thoracic Injury Risk in Frontal Car Crashes with Occupant Restrained with Belt Load Limiter. Society of Automotive Engineers, inc., 983166, 389-401, 1998.
9. Foret-Bruno J-Y, Trosseille X, Page Y, Huere J-F, Le Coz J-Y, Bendjellal F, Diboine A, Phalempin T, Villeforceix D, Baudrit P, Guillemot H, Coltat J-C, Comparison of Thoracic Injury Risk in Frontal Car Crashes for Occupant Restrained without Belt Load Limiters and Those Restrained with 6kN and 4kN Belt Load Limiters, *Stapp Car Crash Journal*, **2001**, 45: 205-224
10. Li, P.; Li, Y.; Hua, X.; Guo, Y.; Curtis, J.S. 3D DEM Simulations and Experiments on Spherical Impactor Penetrating into the Elongated Particles. *Materials* **2023**, 16, 1664. <https://doi.org/10.3390/ma16041664>
11. Mario Buchely, Alejandro Maranon, Spherical Cavity Expansion Approach for the Study of Rigid-Penetrator's Impact Problems, *Appl. Mech.* **2020**, 1, 20–46; doi:10.3390/applmech1010003
12. Jacobo Antona-Makoshi, Yoshihiro Yamamoto, Ryosuke Kato, Shouhei Kunitomi, Atsuhiko Konosu, Yasuhiro Dokko, Tsuyoshi Yasuki, Tomoaki Takamiya, Effect of seatbelt and airbag loads on thoracic injury risk in frontal crashes considering average and small body sizes and age-dependent thoracic fragility, IRCOBI Conference 2016
13. Andre Eggers, Burkhard Eickhoff, Jan Dobberstein, Harald Zellmer, Thorsten Adolph, Effects of Variations in Belt Geometry, Double Pretensioning and Adaptive Load Limiting on Advanced Chest Measurements of THOR and Hybrid III, 2014 IRCOBI Conference, Sep 2014, Berlin, Germany
14. Bingbing Nie, David Poulard, Damien Subit, Jean-Paul Donlon, Jason.L Forman, et al.. Experimental investigation of the effect of occupant characteristics on contemporary seat belt payout behavior in frontal impacts. *Traffic Injury Prevention*, Taylor & Francis, **2016**, 17 (4), pp.374-380. 10.1080/15389588.2015.1088944



15. Bengt Pipkorn, Francisco J. Lopez-Valdes, Christer Lundgren, Dan Bråse, Cecilia Sunnevång, Innovative Seat Belt System for Reduced Chest Deflection., 24th International Technical Conference on the Enhanced Safety of Vehicles (ESV), Gothenburg , Sweden, Date: 8-11.06.2015
16. Philippe Beillas, Anurag Soni, Marie-Christine Chevalier, Q6 Dummy Thoracic Response and Diagonal Belt Interactions: Observations based on Dummy Testing and Human and Dummy Simulations, 2014 IRCOB Conference, Sep 2014, Berlin, Germany
17. Hamid Ghaednia, Xianzhang Wang, Swarna Saha, Yang Xu, A Review of Elastic-Plastic Contact Mechanics, *Applied Mechanics*, **2017**, DOI: 10.1115/1.4038187
18. A. Tiwari, A. Almqvist, B. N. J. Persson, Plastic Deformation of Rough Metallic Surfaces, *Tribology Letters*, **2020**, 68:129, <https://doi.org/10.1007/s11249-020-01368-9>
19. Johnson, K. L., Contact Mechanics, 1987, Cambridge University Press, Cambridge, UK.
20. Ghaednia, H., Pope, S. A., Jackson, R. L., and Marghitu, D. B., A Comprehensive Study of the Elasto-Plastic Contact of a Sphere and a Flat, *Tribol. Int.*, **2016**, 93(Pt. A), pp. 78–90.
21. Alcalá, J., and Esquede los Ojos, D., Reassessing Spherical Indentation: Contact Regimes and Mechanical Property Extractions, *Int. J. Solids Struct.*, **2010**, 47(20), pp. 2714–2732.
22. Quicksall, J. J., Jackson, R. L., and Green, I., 2004, Elasto-Plastic Hemispherical Contact Models for Various Mechanical Properties, *Proc. Inst. Mech. Eng., Part J*, **2004**, 218(4), pp. 313–322.
23. Tabor, D., The Hardness of Metals, 2000, Oxford University Press, New York.
24. Taljat, B., and Pharr, G., Development of Pile-Up During Spherical Indentation of Elastic–Plastic Solids, *Int. J. Solids Struct.*, **2004**, 41(14), pp. 3891–3904.
25. Brinell, J., Way of Determining the Hardness of Bodies and Some Applications of the Same , 1900, Tek. Tidskr., 5, p. 69.
26. Meyer, E., Investigations of Hardness Testing and Hardness, 1908, Z. Phys., 9, pp. 66–74.
27. Chaudhri, M. M., Hutchings, I. M., and Makin, P. L., Plastic Compression of Spheres, *Philos. Mag.*, **1984**, A, 49(4), pp. 493–503.
28. Ye, N., and Komvopoulos, K., Indentation Analysis of Elastic-Plastic Homogeneous and Layered Media: Criteria for Determining the Real Material Hardness, *ASME J. Tribol.*, **2003**, 125(4), pp. 685–691.
29. Komvopoulos, K., and Ye, N., Three-Dimensional Contact Analysis of Elastic-Plastic Layered Media With Fractal Surface Topographies, *ASME J. Tribol.*, **2001**, 123(3), pp. 632–640.
30. R.J.M. Pijpers and H.M. Slot, Friction coefficients for steel to steel contact surfaces in air and seawater, 2020, J. Phys.: Conf. Ser. 1669 012002
31. M. Stembalski, P. Pres, W. Skoczynski, Determination of the friction coefficient as a function of sliding speed and normal pressure for steel C45 and steel 40HM, *Archives of civil and mechanical engineering*, 13, **2013**, 444 – 448.
32. Evin, E.; Daneshjo, N.; Mareš, A.; Tomáš, M.; Petrovčiková, K. Experimental Assessment of Friction Coefficient in Deep Drawing and Its Verification by Numerical Simulation., *Appl. Sci.*, **2021**, 11, 2756. <https://doi.org/10.3390/app11062756>
33. J. J. Arnoux, G. Sutter, G. List, and A. Molinari, Friction Experiments for Dynamical Coefficient Measurement, *Advances in Tribology*, Volume 2011, Article ID 613581, doi:10.1155/2011/613581
34. Rodriguez, S. A., Alcalá, J., and Martins Souza, R., Effects of Elastic Indenter Deformation on Spherical Instrumented Indentation Tests: The Reduced Elastic Modulus, *Philos. Mag.*, **2011**, 91(7–9), pp. 1370–1386.
35. Tabor, D., A Simple Theory of Static and Dynamic Hardness, 1948, Proc.R. Soc. London A, 192(1029), pp. 247–274.
36. www.peninsulardevastagos.es, Steel tubes for precision applications – seamless cold drawn tubes E 235, E355, accessed on 5.11.2020

**Disclaimer/Publisher's Note:** The statements, opinions and data contained in all publications are solely those of the individual author(s) and contributor(s) and not of MDPI and/or the editor(s). MDPI and/or the editor(s) disclaim responsibility for any injury to people or property resulting from any ideas, methods, instructions or products referred to in the content.